

Dynamic Flow Control Through Active Matter Programming Language

Fan Yang,^{1,*} Shichen Liu,¹ Heun Jin Lee,² and Matt Thomson^{1,†}

¹*Division of Biology and Biological Engineering, California Institute of Technology, Pasadena, CA, USA*

²*Department of Applied Physics, California Institute of Technology, Pasadena, CA, USA*

Dynamic networks of cytoskeletal filaments and motor proteins can generate active forces that are essential in many cellular functions, such as cell division, motility, structural support and intracellular transport. Active fluids with such living matter can be chaotic without a control mechanism [1], limiting their utility for bioengineering applications. Recently-developed light-activatable motors, which only crosslink the microtubules under illumination, have been previously applied to still persistent fluid flows [2, 3]. However, the coupled dynamics of active networks and fluid is still poorly understood. Here we construct a coarse-grained model that predicts active matter and fluid flows under dynamic optical input, which shows good agreement with experiments. Using light bars as the basic units, we are able to define the programming language of active matter and create local stretching and mixing flows. In general the flow fields induced by individual bars cannot be linearly superimposed in a composition. Combining theoretical predictions and experimental results, we find that the linear superimposition can be achieved above a critical distance. Therefore, different flows can be realized simultaneously within a single channel through the spatio-temporal composition and manipulation of light patterns, making multitasking possible in a single channel. Our theoretical framework may be extended for other emergent structures of cytoskeleton, and our platform has potentials for building optically programmable flow-control devices.

I. INTRODUCTION

Fueled by ATP hydrolysis, the cytoskeleton and motor proteins can transport organelles [4–6] and create cytoplasmic flows [7–9] at the microscale within a cell. We aim to exploit these biological active matter to build programmable microfluidic devices with high flexibility and precision. Traditional microfluidic techniques for creating desired flows usually require special design of geometries and control of in- and out-let flows, which further demand precise micro-fabrication and pressure pumps of high accuracy [10]. Due to lack of localized control within a channel, each microfluidic channel is usually restricted for a single function. The inadaptability of conventional microfluidics limits its efficiency when a series of operations need to be done. Here we show using light-activatable motors and microtubules, which are only crosslinked under illumination [2], to control the fluid flows through the spatial-temporal design of the optical input. Our system has several advantages over traditional control mechanisms in microfluidics. It provides simple programmable control, with few or no requirements on the channel geometries or precise control of in- and out-let flows. The emergent flows are localized around the light patterns, making it feasible to tackle fine-size localized tasks and integrate different operations in a single channel.

As a proof of concept, using rectangular bars as basic units, we define operations, such as superimposition and rotation, to sculpt stretching and mixing flows, see Fig 1. Within the rectangular illuminated region, microtubules are dynamically crosslinked into a contracting network [2] that functions as a microfluidic pump, which absorbs fluid lengthwise and pump it out widthwise (Fig 1a) [3]. When two light bars are superimposed along the lengthwise direction, there is an extensional flow at the gap between them (Fig 1b). When the optical bar rotates, the flow field, consisting of four counter-rotating vortices, also rotates with the light bar and mixes its surrounding area (Fig 1c).

To understand the non-equilibrium behaviors of the active matter and predict flow fields, we build a continuum model quantifying the coupled dynamics of microtubules and fluid. Active networks of microtubules and motors exhibit diverse, and sometimes seemingly contradictory, behaviors under different conditions [11, 12]. For example, both contractile [2, 13] and extensile [14] microtubule gels have been observed. Classified by symmetry, microtubule networks can exist in isotropic [3], polar [15] or nematic [14, 16] states. The active contraction in our system is mainly driven by the number density difference of dimerized motors and microtubules, where the isotropic contractile forces are the central driving force. Indeed, such forces have been found to induce the active contraction of microtubule stripes [13]. In terms of theories, coarse-grained models have been derived based on thermodynamic principles, such as the active gel theory [17–19], or microscopic interactions of motors and microtubules [20–22]. However, direct comparison of models and experiments for both microtubules and the ambient fluid is still lacking. Past attempts at

* E-mail: fy2@caltech.edu

† E-mail: mthomson@caltech.edu

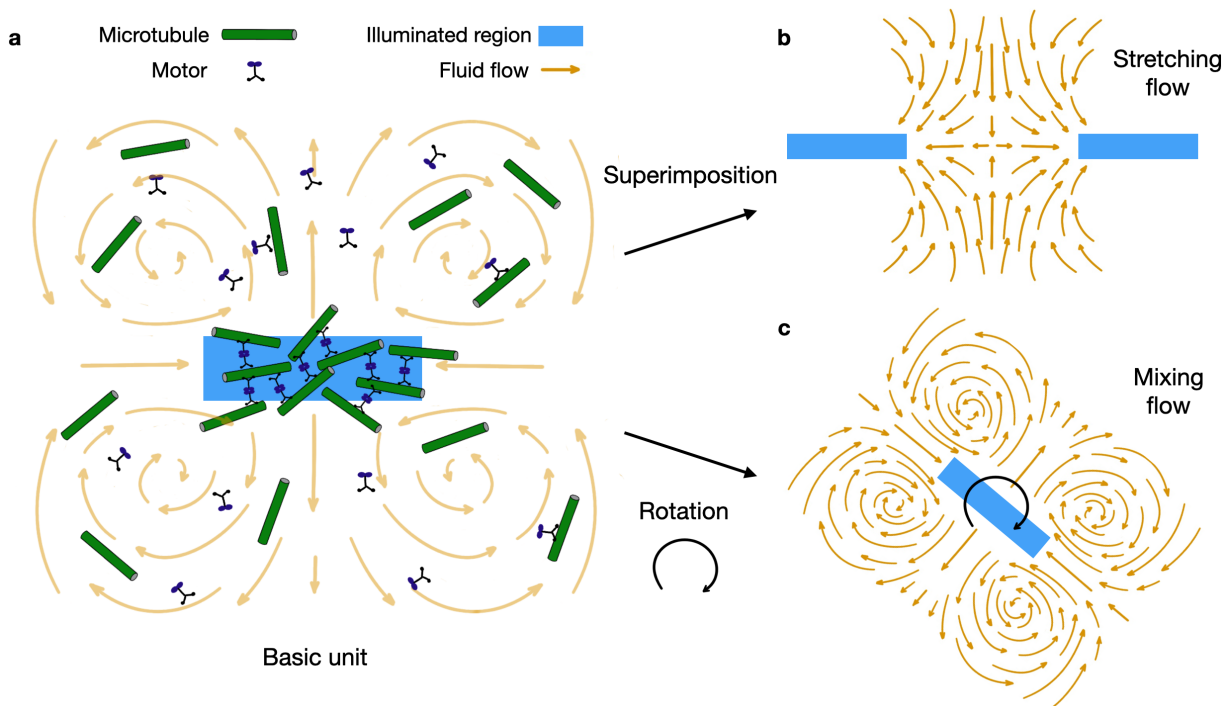


FIG. 1: Manipulation of rectangular light patterns provides a potential strategy for active-matter-driven fluid-flow control. **a.** The light-activatable motors dimerize under illumination and crosslink the microtubules into a dense network [2]. The motion of microtubules drives a flow of the background solution. For a rectangular light bar, the fluid flows into the shorter sides and out of the longer sides, forming four counter-rotating vortices [3]. **b.** Superimposition of two light bars can generate an extensional flow at the gap between them, where the flow is stretched along the lengthwise direction. **c.** When the optical bar rotates, the four vortices also rotate following the light bar and mix the surround region. Motors and microtubules are not drawn in **b** and **c**.

modeling fluid flows in our system is mainly through the boundary force model [2, 3], by placing force singularities at the boundaries of the illuminated region. The singularities are assumed immobile and thus the dynamics of active microtubules is not captured with this approach. In this paper, we propose a coarse-grained model based on the microscopic interactions of microtubules and motors, together with first principles of fluid mechanics. In particular, we explicitly model the reversible dimerization and binding kinetics of the motors and consider the mechanical properties of the active networks dependent on the concentration of the bound motors.

II. RESULTS

Our system consists of stabilized microtubules, engineered kinesin motor proteins [2] and ATP, placed in a Hele-Shaw cell. Light pulses of 470 nm, which activates the motor dimerization, are projected onto the cell every 5 seconds (Materials and Methods). Dimer motors can crosslink microtubules into an active network within the illuminated region [2]. Dynamic control of active networks and consequent fluid flows is achieved by spatio-temporal modulation of the optical signals.

When the light signal consists of two rectangles (Fig 2a), an extensile fluid flow can develop at the gap between them, which is stretching along the lengthwise direction (Fig 2b). When the two light bars are relatively widely separated (Fig 2a), the flow directions are quasi-steady (Fig 2b) with a varying magnitude in time. This flow field can be approximately deemed as a linear superimposition of the flows induced by each individual light bar [3]. However, when the gap width between the two light bars is below a critical value, the two networks will move to the gap center and eventually merge (Fig2c). The consequent flow field is highly dynamic. One hypothesis for the merging of active networks can be the hydrodynamic interactions between them. Since each network absorbs fluid along the lengthwise direction, the overall hydrodynamic interactions are attractive in this direction.

We build a continuum model to verify this hypothesis. In terms of mechanics, our model is essentially a three-phase

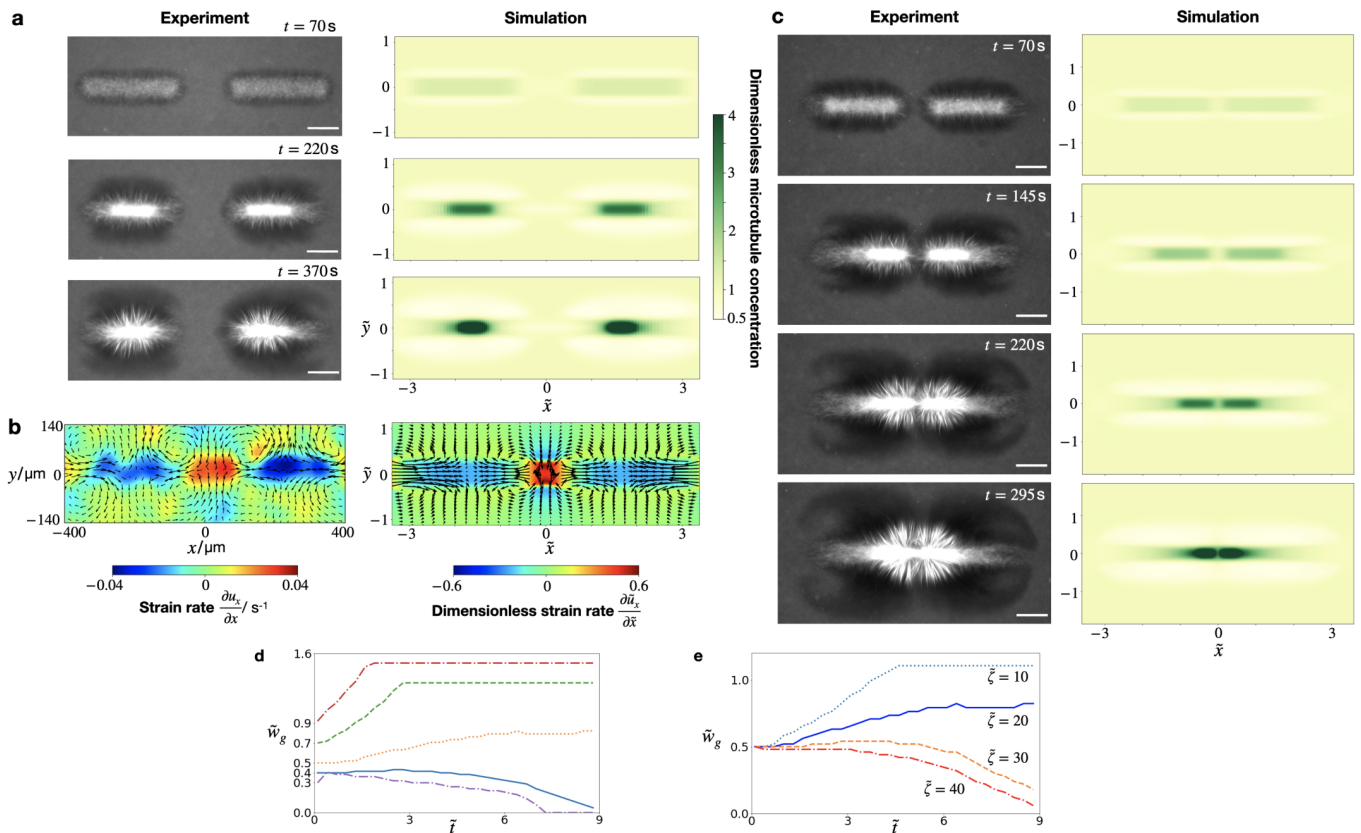


FIG. 2: Composition of static rectangular bars provides quantitative programming primitive for generating stretching flows. **a.** Time-lapse images of the microtubule networks in experiments and simulations. The heat map in the simulations shows the total microtubule concentration, i.e., the sum of crosslinked and freely-moving microtubules. **b.** Typical fluid flow field generated in **a.** The flow in the gap is a stretching flow along x -direction. **c.** Time-lapse images of the merging of active networks when the initial gap width is small. **d.** Simulation results for the time evolution of the gap widths with different initial conditions labeled on the y -axis. For initial gap widths smaller than a critical value, around 0.5 for this set of parameters, the two active networks will merge. **e.** Simulation results for the time evolution of gap widths with different flow intensities. Increasing $\tilde{\zeta}$ will increase the flow intensity and enhance the tendency of merging. This shows that the merging effects is mainly due to the hydrodynamic attraction of active networks. All scale bars are $100 \mu\text{m}$ and all simulations are dimensionless.

complex fluids model and the three phases are crosslinked microtubules, freely-moving (uncrosslinked) microtubules and the solvent fluid. The crosslinked microtubules are modeled as a viscoelastic gel, which self-contracts by its internal active stresses. The freely-moving microtubules follow the motions of the gel and the fluid and the resultant velocity is determined by the competition between the frictions with the gel and fluid. The fluid flow is in turn driven by the frictions with microtubules and balanced by the hydrodynamic resistance in the Hele-Shaw cell. Other chemical species in our model include monomer motors, freely-moving (unbound) dimer motors, bound dimer motors, and ATP. We explicitly calculate the reversible crosslinking of microtubules, reversible dimerization and binding of motors, and consumption of ATP through their continuity equations.

The momentum equation of the viscoelastic microtubule gel is

$$\nabla \cdot (\boldsymbol{\sigma}_a + \boldsymbol{\sigma}_v + \boldsymbol{\sigma}_{el} + \boldsymbol{\sigma}_{st}) + \mathbf{f}_{fl} + \mathbf{f}_f = \mathbf{0}, \quad (1)$$

where $\boldsymbol{\sigma}_a$, $\boldsymbol{\sigma}_v$, $\boldsymbol{\sigma}_{el}$ and $\boldsymbol{\sigma}_{st}$ are the active, viscous, elastic and steric stresses in the gel, \mathbf{f}_{fl} and \mathbf{f}_f are the frictions with the fluid and freely-moving microtubules, respectively. Their explicit expressions can be derived from microscopic interactions based on previous work [21, 22], see full derivations in the Supplemental Information. The active contractile stress is

$$\boldsymbol{\sigma}_a = \alpha c_A d_b c \mathbf{I}, \quad (2)$$

where c , c_A and d_b are the concentrations of the crosslinked microtubules, ATP and the bound dimer motors, respectively, α is a constant activity coefficient and \mathbf{I} is the identity tensor. In general, the active stresses can have isotropic, polar and nematic components [11, 22]. In our experiments, the contraction of networks is found to be mainly isotropic [3]. Therefore, the isotropic contractile stress is assumed to dominate in this process, especially when the microtubule networks are not densely crosslinked. The viscous stress is $\boldsymbol{\sigma}_v = \eta d_b c (\nabla \mathbf{v} + \nabla \mathbf{v}^T)$, where \mathbf{v} is the velocity of the crosslinked microtubules and η is the viscosity coefficient. The elastic stress $\boldsymbol{\sigma}_{el}$ is assumed to follow the Maxwell model with a long relaxation time [23],

$$\frac{D\boldsymbol{\sigma}_{el}}{Dt} - [\boldsymbol{\sigma}_{el} \cdot \nabla \mathbf{v} + \nabla \mathbf{v}^T \cdot \boldsymbol{\sigma}_{el}] = \eta_{el} d_b c (\nabla \mathbf{v} + \nabla \mathbf{v}^T) - p^u \boldsymbol{\sigma}_{el}, \quad (3)$$

where t is the time, η_{el} is the elasticity coefficient and p^u is the un-crosslinking rate of the gel. We note that the affects of the bound motor density on the active stress and mechanical properties of the gel are highly non-trivial [24], especially in our experiments where the active contraction is mainly driven by the concentration difference of the bound motors in and outside the illuminated regions. The steric stress is $\boldsymbol{\sigma}_{st} = -\xi c^2 \mathbf{I}$. The friction with freely-moving microtubules is $\mathbf{f}_f = \beta_f c c_f (\mathbf{v}_f - \mathbf{v})$ where c_f is the freely-moving microtubule concentration, \mathbf{v}_f is the velocity, and β_f is the friction coefficient. The friction with fluid is $\mathbf{f}_{fl} = \gamma c (\mathbf{u} - \mathbf{v})$ with the fluid velocity \mathbf{u} and the drag coefficient γ . In general the hydrodynamic drag coefficient depends on the fiber orientation [25], in this paper we neglect the polarity in both active stresses and hydrodynamic frictions.

We assume the freely-moving microtubules only experience frictions from the gel and the ambient fluid. The force balance is $\beta_f c c_f (\mathbf{v} - \mathbf{v}_f) + \gamma c_f (\mathbf{u} - \mathbf{v}_f) = \mathbf{0}$, and their velocity is therefore $\mathbf{v}_f = (\beta_f c \mathbf{v} + \gamma \mathbf{u}) / (\beta_f c + \gamma)$.

The fluid flow in the Hele-Shaw cell has the form of the Darcy's law with additional contributions from the microtubule frictions. The averaged two-dimensional fluid flow is

$$\mathbf{u} = -\frac{h^2}{12\mu} [\nabla \Pi + (\gamma c + \gamma_f c_f) (\mathbf{u} - \mathbf{v})], \quad (4)$$

with h the height of channel, μ the fluid viscosity, Π the fluid pressure and $\gamma_f = \gamma \beta_f c / (\beta_f c + \gamma)$.

The transport equation for the monomer motor proteins is

$$\frac{\partial m}{\partial t} + \nabla \cdot (m \mathbf{u}) = 2(p^m d_f - p^d m^2) + D_m \nabla^2 m, \quad (5)$$

where m is the monomer motor concentration, d_f is the freely-moving dimer concentration, D_m is the diffusivity, p^m and $p^d(x, y, t)$ are the monomerization and dimerization rates, respectively. The monomer motors are assumed to follow the fluid flow and therefore $\nabla \cdot (m \mathbf{u})$ is the convective term. We assume $p^d(x, y, t)$ is proportional to the light intensity. Thus the light signals are implemented through spatio-temporal arrangement of $p^d(x, y, t)$ in our model, see details in the Appendix A. Continuity equations of other species are listed in the Appendix A.

Equations (1-5) and (A1-A5) are numerically solved using finite difference methods to predict the microtubules and fluid flows in response to the optical input. In simulations (Fig 2), the two microtubule networks also merge when the initial gap width is small (Fig 2c). We plot the time evolution of the non-dimensionalized gap width \tilde{w}_g in Fig 2c, which confirms that there is a critical value for the initial gap width under which the two networks will merge. To further verify this merging is due to hydrodynamic interactions, we vary the fluid flow magnitudes in simulations. To achieve this, we first non-dimensionalize our governing equations, and the dimensionless version of the fluid equation (4) is

$$\tilde{\mathbf{u}} = -\tilde{\zeta} \left[\tilde{\nabla} \cdot \tilde{\Pi} + \frac{\beta_f c}{\beta_f c + \gamma} (\tilde{\mathbf{u}} - \tilde{\mathbf{v}}) \right], \quad (6)$$

where all variables with a tilde on top are dimensionless. The flow intensity increases with the dimensionless parameter $\tilde{\zeta} = c_0 \gamma h^2 / 12\mu$, where c_0 is the initial microtubule concentration. The time evolution of gap widths for different $\tilde{\zeta}$ are plotted in Fig 2e. We can see that there is an increasing tendency of merging with higher fluid flow intensity. This shows that the merging of active networks is indeed due to their hydrodynamic attraction.

When the optical signal is a rotating bar, the flow field, consisting of four vortices, also rotates following the light pattern, as shown in Fig 3a and 3b. Our simulations can predict the structures of both the microtubules and the fluid flow. As the light bar rotates, the microtubule gel dynamically forms and self-contracts into a core. As the light bar is shed on a new location from one pulse to the next, two plumes of newly-crosslinked microtubules are formed at the ends of the gel, which transport both mass and momentum of microtubules to the network core, as well as rotates the more densely-crosslinked network center. After one cycle, the circular region swept by the light bar will be mixed by the rotating vortices. The rotational speed of the light bar is 2° per light pulse in Fig 3a and 3b. Typically we want

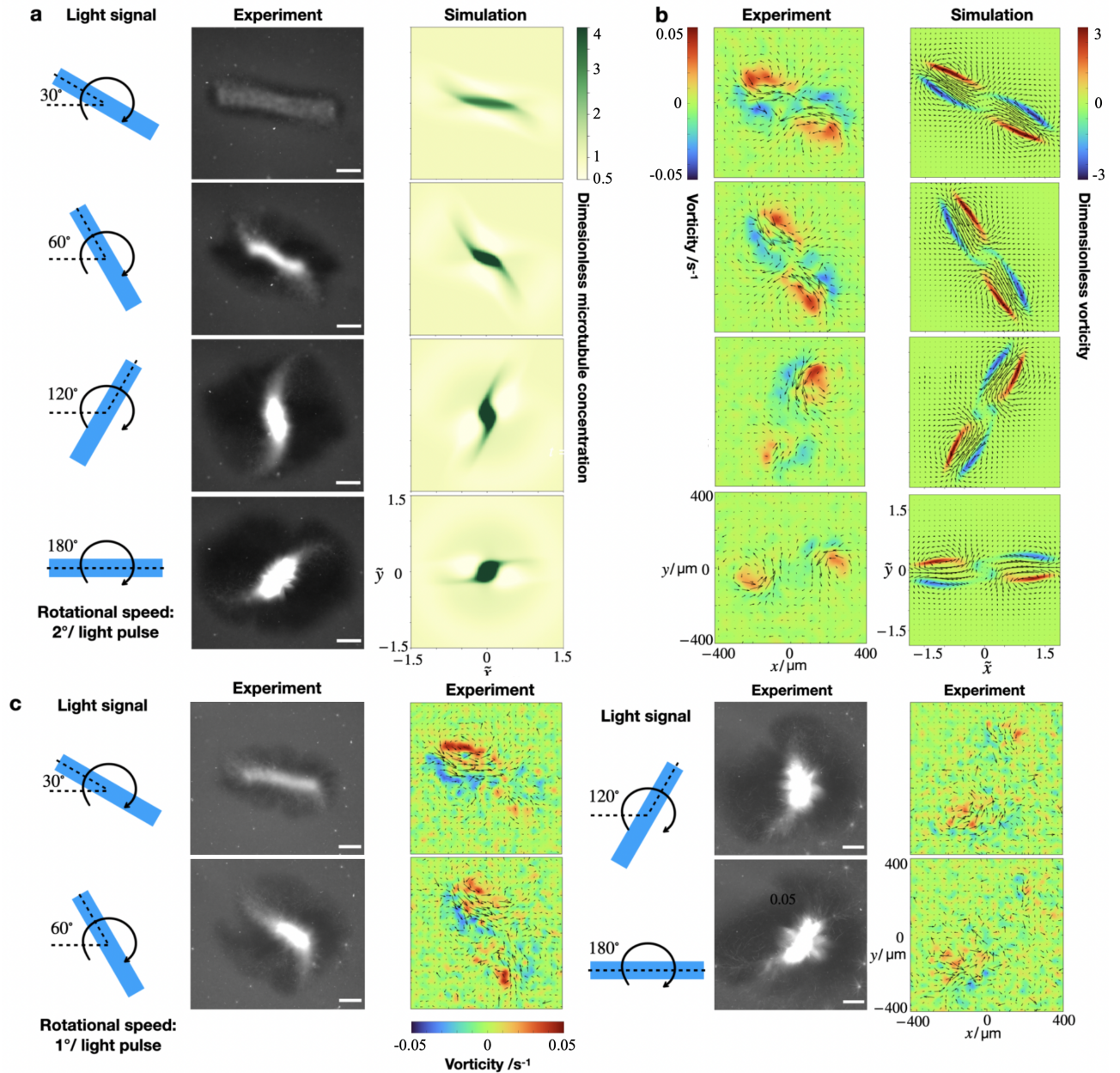


FIG. 3: **Rotation of light bars can generate local mixing flows. The mixing efficiency is tuned by the rotational speed of the bar.** Time-lapse images of **a.** microtubule networks and **b.** flow fields in experiments and simulations. The rotational speed of the light bar is 2° per light pulse. Within one cycle, the four vortices rotate following the light bar and stir the circular region swept by it. **c.** When the rotational speed is 1° per light pulse, both the active gel and the fluid flow become unstable.

the light bar to rotate slowly to stir well its surrounding region. However, when the rotational speed is too small, both the microtubule network and flow field can become unstable, as shown in Fig 3c, where the rotational speed is 1° per light pulse. Experimentally, a slower rotating light bar will generate a more densely-crosslinked microtubule gel, and this instability may be caused by the percolation effects of the active gel [26]. In experiments we find that under a static light bar, the microtubule network self-contracts to a core. Once the network is densely crosslinked, it is impossible to rotate this core with a rotating light bar. So the highly-crosslinked gel is unresponsive to a rotating light bar. The static light bar can be deemed as a limit case where the rotating bar has a 0 rotational speed. For a rotational speed of 2° per light pulse, the microtubule gel rotates well following the bar. Therefore the unstable dynamics under 1° per light pulse may be at an intermediate regime where the microtubule gel is partly responsive

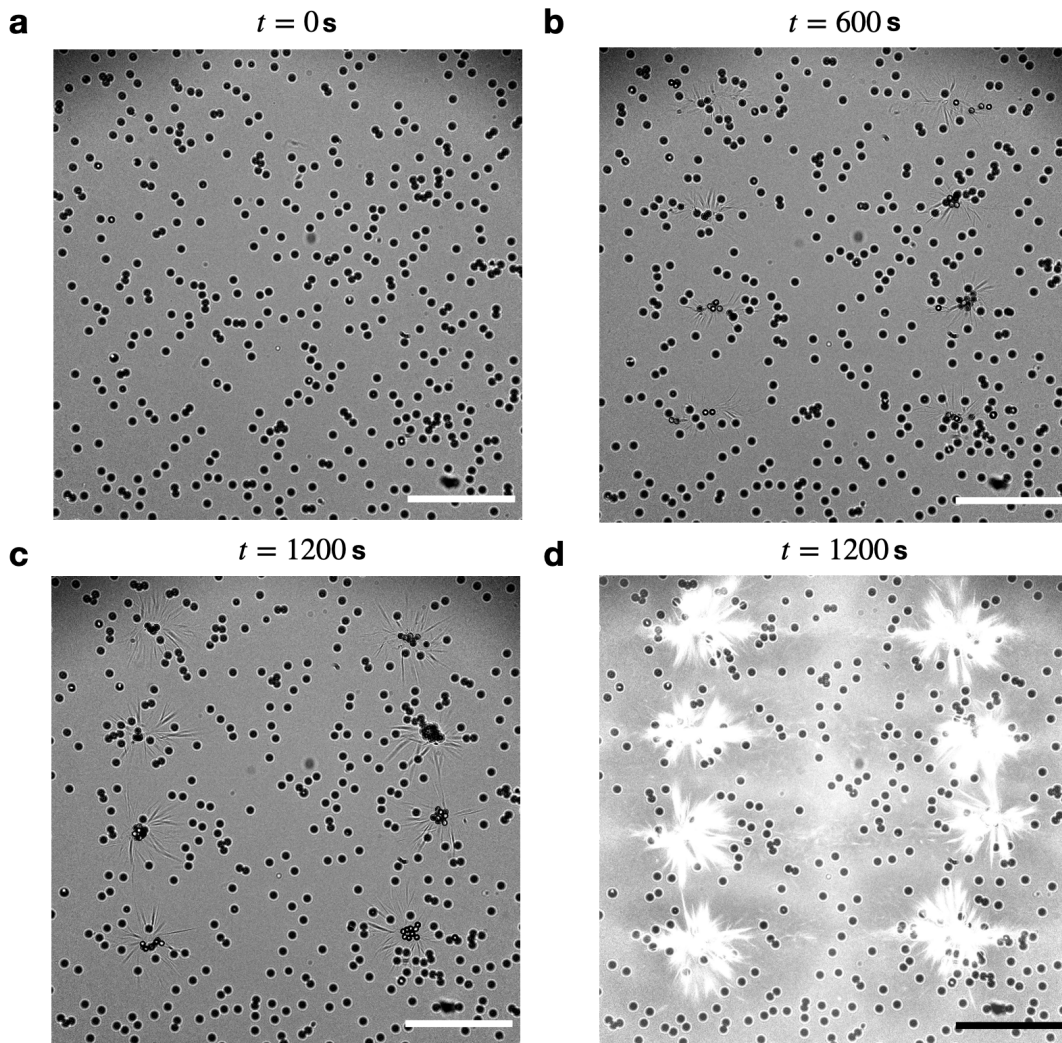


FIG. 4: **Above a critical length scale, bar superposition enables model-driven design of macroscopic flow fields that allows for simultaneous multi-tasking in a single channel. For example, composition of static bars can move particles onto a lattice set by the bar centers.** **a-c.** Time-lapse images of particles moving to the network centers. The seemingly larger and darker particles are those sitting on the channel bottom and therefore less prone to the fluid flow. **d.** Image of microtubules networks and particles. All scale bars are $200 \mu\text{m}$ and the particles are around $10 \mu\text{m}$ in diameter.

to the rotation of the light signal.

Composition of light patterns can drive macroscopic flows and move particles. In Fig 4, we show an example where two arrays of microtubule networks is formed in a solution of $10\text{-}\mu\text{m}$ -diameter passive particles. The particles at the image plane are moved to lattice defined by the network centers (Fig 4 a-c). The seemingly bigger and darked particles in Fig 4 are much less mobile because they are close to the bottom of the channel where the fluid flow is weak. It is of note that an electronically programmable microfluidic control device is proposed recently [27], which is driven by artificial cilia and more effective at creating flows near the channel surface, whereas our system is more efficient in driving flows near the channel center.

III. DISCUSSION

Microfluidic devices are extensively used in science and technology. Our bio-inspired platform provides a potential strategy for optically programmable control of microfluidic flows. Using engineered motor proteins and microtubules, we can generate desired fluid flows by spatio-temporal modulation of light input. Flows induced by composition of

light patterns are approximately mutually unaffected when their spacing is above a critical value, making it possible for linear superimposition and multi-tasking in a single channel.

A quantitative coarse-grained theory is derived for model-driven design of flow fields. We find it crucial to classify the microtubules into two phases by whether they are crosslinked or not. The crosslinked microtubule network can be well modeled as a viscoelastic gel with an isotropic contractile stress. The mechanical properties of the gel depend on its own density and also the concentration of the bound motors. Since our model couples the dynamics of both the microtubules and the fluid, we uncover that the merging of two adjacent active networks is mainly due to their hydrodynamic attraction. The theory shows that the induced fluid flow intensity depends on the dimensionless parameter $\tilde{\zeta} = c_0\gamma h^2/12\mu$, which is the ratio of the driving force, i.e., frictions from microtubules, and the hydrodynamic resistance in the Hele-Shaw cell. This is promising in applications because the flow intensity increases with the height of the channel, and consequently larger fluid volume. The model also successfully predicts results under dynamic light signals, such as a rotating bar. Our theory provides a general framework for active microtubules and fluid, which may be applied to other out-of-equilibrium structures of cytoskeleton.

ACKNOWLEDGMENTS

We acknowledge funding from The Packard Foundation, The Moore Foundation, National Institute of Health and the Donna and Benjamin M. Rosen Bioengineering Center. F. Y. acknowledges support from the BBE Divisional Fellowship at Caltech.

Appendix A: Continuity Equations

In this Appendix we list all the continuity equations that are not included in the main text. The continuity equations for the crosslinked and freely-moving microtubules are

$$\frac{\partial c}{\partial t} + \nabla \cdot (c\mathbf{v}) = p_1^{on} c_f d_f - p^u c, \quad (\text{A1a})$$

$$\frac{\partial c_f}{\partial t} + \nabla \cdot (c_f \mathbf{v}_f) = -p_1^{on} c_f d_f + p^u c + D_f \nabla^2 c_f. \quad (\text{A1b})$$

where p_1^{on} is the crosslinking rate, p^u is the un-crosslinking rate and D_f is the diffusivity of the freely-moving microtubules.

The transport equation for the monomer motors is (5). The continuity equations for the freely-moving and the bound dimer motors are

$$\frac{\partial d_f}{\partial t} + \nabla \cdot (d_f \mathbf{u}) = -p^m d_f + p^d m^2 - p_1^{on} c_f d_f - p_2^{on} c d_f + p^{off} d_b + D_d \nabla^2 d_f \quad (\text{A2a})$$

$$\frac{\partial d_b}{\partial t} + \nabla \cdot (d_b \mathbf{v}) = p_1^{on} c_f d_f + p_2^{on} c d_f - p^{off} d_b, \quad (\text{A2b})$$

where p^m is the monomerization rate, p_2^{on} is the rate of the dimer motors binding on the already-crosslinked microtubules, p^{off} and d_b are the unbinding rate and the concentration of the bound dimers, respectively, D_d is the diffusivity of the free dimers and $p^d(x, y, t)$ is the dimerization rate, assumed to be proportional to the light intensity. For a static rectangular light bar, $p^d(x, y, t)$ has the form of

$$p^d(x, y, t) = \frac{p_0^d}{\left(1 + \left(\frac{x-c_x}{r_x}\right)^{12}\right) \left(1 + \left(\frac{y-c_y}{r_y}\right)^{12}\right)}, \quad (\text{A3})$$

which is approximately a rectangular function with its center at (c_x, c_y) , side lengths $2r_x$ and $2r_y$, and maximum value p_0^d . The exponent “12” is empirically chosen. In general this exponent should be an even number and a larger exponent yields a sharper boundary of the rectangle. For a rotating light bar, one just needs to rotate the above equation in the $x - y$ plane for different t .

The transport equation for the ATP is

$$\frac{\partial c_A}{\partial t} + \nabla \cdot (c_A \mathbf{u}) = -k_A d_b c_A + D_A \nabla^2 c_A, \quad (\text{A4})$$

where k_A is the consumption rate of the ATP by the bound dimer motors, and D_A is the ATP diffusivity. The continuity equation for the solvent fluid is

$$\nabla \cdot \mathbf{u} = 0. \quad (\text{A5})$$

Appendix B: Materials and Methods

Kinesin Purification, Microtubule Polymerization, and Chamber Construction. Kinesin purification, microtubule polymerization and chamber construction were described in previous work [2]. In short, we constructed and purified two kinesin K401 with light-induced hetero-dimer system of iLID and SspB-micro: K401-iLID and K401-micro. For protein expression, we transformed the plasmids into BL21pLysS cells and induced the cells with IPTG. For protein purification, we lysed the cells and used Ni-NTA agarose resin to pick up His tags that were provided by the base plasmids. MBP domain was used and subsequent cleaved off in K401-micro expression to ensure the micro domain remains fully functional during expression.

Tubulin was polymerized with the non-hydrolysable GTP analog GMP-CPP [28]. Labelled and unlabeled tubulin were palleted and then incubated at 37°C to form GMP-CPP stabilized microtubules. We then characterized the microtubule length distribution by immobilizing them onto cover glass surface using poly-L-lysine.

The chambers were made from microscope slides and cover slips that were passivated against non-specific protein binding with a hydrophilic acrylamide coating [29]. A flow cell made with pre-cut parafilm was used to seal between the microscope slides and coverslips making a channel that is about 70 μm in height. After the addition of reaction mixture, the flow cells were sealed with dental silicone polymer.

Energy Mixture and Reaction Mixture. An energy mix consisting an energy source (ATP), a crowding agent (glycerol), a surface passivating reagent (pluronic acid), oxygen scavengers (glucose oxidase, glucose, catalase, Trolox, and DTT) and ATP-recycling reagents was made on ice prior to combining the motor proteins and microtubules. After equilibrating the energy mix to ambient temperature, K401-micro, K401-iLID and microtubules were combined with the energy mix into a reaction mix. Concentrations for protein monomers for the K401-micro and K401-iLID constructs were 0.1 μM , and for microtubules, 1.5 – 2.5 μM . To minimize unintended light activation and non-specific protein binding, the sample was prepared under dark-room conditions with filters to block wavelengths below 580 nm. M2B pH 6.1 spike-in should also be minimized to avoid non-specific micro-iLID binding.

Tracer Beads Preparation. To visualize the fluid dynamics of our system, we used 1 μm polystyrene beads as tracer particles. The particles were incubated overnight in M2B pH6.8 buffer with 50 mg/ml pluronic acid. The beads were then washed and palleted at 1000xg for 2 minutes and resuspended in M2B pH 6.8 before adding them into the reaction mix.

Design and Implementation of Different Bar Patterns. We custom fitted an epi-illuminated pattern projector onto our microscope. The size of the projection field is 800 x 1280 pixels. Bar dimension in all experiments was 300 x 50 pixels with the exception of rotating bar at 500 x 80 pixels and bar array at 150 x 25 pixels. Matrices containing coordinates of bars were first computed in Python and then converted to greyscale and eventually saved into tiff formats.

Data Acquisition and Projection of Patterns. All experiments were performed with an automated widefield epifluorescence microscope with custom epi-illuminated projector and LED gated transmitted light discussed in our previous work [2]. All samples were imaged at 10X magnification. Images of the fluorescent microtubules (cy5) and tracer particles (brightfield) were also acquired every 5 seconds. Bar patterns are projected onto the image plane every 5 seconds with a brief 50 – 200 milliseconds flash of a 2.4 mW/mm² activation light from a 470 nm LED. The durations of activation lights were empirically determined by gradually increase or decrease the activation time based on the activity of the samples.

Numerical Simulation. The finite difference method was used in numerical simulations with the central differencing scheme in space and the method of lines in time. The velocity fields of the gel and fluid, denoted by \mathbf{v} and \mathbf{u} , respectively, are coupled in the momentum equations (1) and (4). At each time step, we used iterations to solve \mathbf{v} and \mathbf{u} .

-
- [1] K. T. Wu, J. B. Hishamunda, D. T. N. Chen, S. J. DeCamp, Y. W. Chang, A. Fernández-Nieves, S. Fraden, and Z. Dogic, Transition from turbulent to coherent flows in confined three-dimensional active fluids, *Science* **355**, eaal1979 (2017).
 [2] T. D. Ross, H. J. Lee, Z. Qu, R. A. Banks, R. Phillips, and M. Thomson, Controlling organization and forces in active matter through optically defined boundaries, *Nature* **572**, 224 (2019).

- [3] Z. Qu, D. Schildknecht, S. Shadkhoo, E. Amaya, J. Jiang, H. J. Lee, D. Larios, F. Yang, R. Phillips, and M. Thomson, Persistent fluid flows defined by active matter boundaries, *Commun. Phys.* **4**, 198 (2021).
- [4] W. E. Theurkauf, S. Smiley, M. L. Wong, and B. M. Alberts, Reorganization of the cytoskeleton during *Drosophila* oogenesis: implications for axis specification and intercellular transport, *Development* **115**, 923 (1992).
- [5] R. D. Vale, The molecular motor toolbox review for intracellular transport, *Ann. Rev. Cell Biol.* **112**, 467 (2003).
- [6] N. Hirokawa, Y. Noda, Y. Tanaka, and S. Niwa, Kinesin superfamily motor proteins and intracellular transport, *Nat. Rev. Mol. Cell Biol.* **10**, 682 (2009).
- [7] N. Kamiya, Physical and chemical basis of cytoplasmic streaming, *Ann. Rev. Plant Physiol.* **32**, 205 (1981).
- [8] D. Needleman and M. J. Shelley, The stormy fluid dynamics of the living cell, *Phys. Today* **72**, 32 (2019).
- [9] D. B. Stein, G. D. Canio, E. Lauga, M. J. Shelley, and R. E. Goldstein, Swirling instability of the microtubule cytoskeleton, *Phys. Rev. Lett.* **126**, 028103 (2021).
- [10] H. A. Stone, A. Stroock, and A. Ajdari, Engineering flows in small devices: Microfluidics toward a lab-on-a-chip, *Annu. Rev. Fluid Mech.* **36**, 381 (2004).
- [11] M. Marchetti, J. F. Joanny, S. Ramaswamy, T. B. Liverpool, J. Prost, M. Rao, and R. A. Simha, Hydrodynamics of soft active matter, *Rev. Mod. Phys.* **85**, 1143 (2013).
- [12] D. Needleman and Z. Dogic, Active matter at the interface between materials science and cell biology, *Nat. Rev. Mater.* **2**, 17048 (2017).
- [13] P. J. Foster, S. Fürthauer, M. J. Shelley, and D. J. Needleman, Active contraction of microtubule networks, *eLife* **4**, e10837 (2015).
- [14] T. Sanchez, D. T. N. Chen, S. J. DeCamp, M. Heymann, and Z. Dogic, Spontaneous motion in hierarchically assembled active matter, *Nature* **491**, 431 (2012).
- [15] B. A. Dalton, D. Oriola, F. Decker, F. Jülicher, and J. Brugués, A gelation transition enables the self-organization of bipolar metaphase spindles, *Nat. Phys.* **18**, 323 (2022).
- [16] S. J. DeCamp, G. S. Redner, A. Baskaran, M. F. Hagan, and Z. Dogic, Orientational order of motile defects in active nematics, *Nat. Mater.* **14**, 1110 (2015).
- [17] J. F. Joanny, F. Jülicher, K. Kruse, and J. Prost, Hydrodynamic theory for multi-component active polar gels, *New J. Phys.* **9**, 422 (2007).
- [18] J. Prost, J. F. Joanny, and F. Jülicher, Active gel physics, *Nat. Phys.* **11**, 111 (2015).
- [19] F. Jülicher, S. W. Grill, and G. Salbreux, Hydrodynamic theory of active matter, *Rep. Prog. Phys.* **81**, 076601 (2018).
- [20] A. Ahmadi, M. C. Marchetti, and T. B. Liverpool, Hydrodynamics of isotropic and liquid crystalline active polymer solutions, *Phys. Rev. E* **74**, 061913 (2006).
- [21] S. Fürthauer, B. Lemma, P. J. Foster, S. C. Ems-McClung, C. H. Yu, C. E. Walczak, Z. Dogic, D. J. Needleman, and M. J. Shelley, Self-straining of actively crosslinked microtubule networks, *Nat. Phys.* **15**, 1295 (2019).
- [22] S. Fürthauer, D. J. Needleman, and M. J. Shelley, A design framework for actively crosslinked filament networks, *New J. Phys.* **23**, 013012 (2021).
- [23] M. Alves, P. Oliveira, and F. Pinho, Numerical methods for viscoelastic fluid flows, *Annu. Rev. Fluid Mech.* **53**, 509 (2021).
- [24] S. Fürthauer and M. J. Shelley, How cross-link numbers shape the large-scale physics of cytoskeletal materials, *Annu. Rev. Condens. Matter Phys.* **13**, 365 (2022).
- [25] L. G. Leal, *Advanced Transport Phenomena* (Cambridge University Press, 2007).
- [26] J. Alvarado, M. Sheinman, A. Sharma, F. C. MacKintosh, and G. H. Koenderink, Force percolation of contractile active gels, *Soft Matter* **13**, 5624 (2017).
- [27] W. Wang, Q. Liu, I. Tanasijevic, M. F. Reynolds, A. J. Cortese, M. Z. Miskin, M. C. Cao, D. A. Muller, A. C. Molnar, E. Lauga, P. L. McEuen, and I. Cohen, Cilia metasurfaces for electronically programmable microfluidic manipulation, *Nature* **605**, 681 (2022).
- [28] N. Georgoulia, Tubulin Polymerization with GTP/GMPCPP/Taxol, (2012).
- [29] A. W. C. Lau, A. Prasad, and Z. Dogic, Condensation of isolated semi-flexible filaments driven by depletion interactions, *EPL* **87**, 48006 (2009).